Supplement of Atmos. Chem. Phys., 20, 9821–9835, 2020
https://doi.org/10.5194/acp-20-9821-2020-supplement

Atmospheric Chemistry and Physics
Open Access
EGU

Supplement of

Probing key organic substances driving new particle growth initiated by iodine nucleation in coastal atmosphere

Yibei Wan et al.

Correspondence to: Huan Yu (yuhuan@cug.edu.cn)

Text:

ESI-FT-ICR MS operation conditions

Figures:

Figure S1: Figure S1. (a) The observation site, indicated as a red star, in an aerial photograph. Photo source: Baidu Map. (b) 72-hour air mass back trajectories ending at 100 m above ground level at the observation site computed by HYSPLIT model during the I-NPF events from May 8 to 10, 2018.

Figure S2. (a), (c) Number concentration of 2-7 nm particles ($N_{2\text{-}7}$), tidal height and solar radiation intensity during the Iodine-initiated NPF (I-NPF) days from May 9 to 11 and the continental regional NPF (C-NPF) days from February 11 to 13. Particle number size distribution and 10-56 nm particle mass concentration during (b) I-NPF days from May 9 to 11, (d) C-NPF days from February 11 to 13 and (e) non-NPF days from April 16 to 18.

Figure S3. Reconstructed mass spectra of the 7 elemental groups in ESI-and ESI+ modes for the four size bins.

Figure S4: DBE vs. C atom number diagrams of all the CHON and CHO formulas detected in 10–18 nm particles in ESI+ mode. (a) (b) +H adducts, (c) (d) +Na adducts. The color bar denotes the O number in the formulas. The size of the circles reflects the relative intensities of molecular formulas on a logarithmic scale.

Figure S5: Relative intensities of subgroups according to O atom number in CHON, CHO, CHONI and CHOI formulas in the four size bins in ESI+ (in red) and ESI- (in blue). The intensity of the most abundant subgroup is defined as 1 and those of other subgroups are normalized by it. The relative intensities of non-iodinated OC formulas (iodinated OC formulas) are plotted in the region above (below) zero line.

Figure S6: O atom number of *vs.* N atom number of $C_{10}H_xO_yN_z$ compounds detected in 180–560 nm particles (a) and $C_{18}H_xO_yN_z$ compounds detected in 10–18 nm particles in ESI- mode (b).

Figure S7: Simplified reaction scheme showing the formation of oxygenated and nitrated CHO and CHON compounds from α-linolenic acid oxidation in the atmosphere.

Figure S8: Simplified reaction scheme showing the formation of oxygenated CHO compounds from unsaturated C_{28} FA ($C_{28}H_{52}O_2$) oxidation in the atmosphere.

Figure S9: Simplified reaction scheme showing the formation of oxygenated CHON compounds containing a –NH_2 group from unsaturated C_{18} amino alcohol ($C_{18}H_{37}NO_4$) oxidation in the atmosphere.

Tables:

Table S1. Predicted saturation concentration (C*) range of most abundant CHON and CHO formulas, as well as their possible precursors.

ESI-FT-ICR MS operation conditions

A syringe pump infused the sample extract continuously into the ESI unit with a flow rate of 180 μL h-1. The ESI source conditions were as follows: the nebulizer gas pressure was 1 bar; the dry gas (N_2) pressure was 4 bar and its temperature was 200 ℃; the capillary voltage was 4.5 kV. The ion accumulation time in the argon-filled hexapole collision pool with 1.5 V of direct current voltage and 1400 Vp-p of radio frequency (RF) amplitude was 0.05 s, followed by transport ions through a hexapole ion guide to the ICR cell for 0.7 ms. 4 M words of data were recorded over the mass range of 150-1000 for each run. A total of 128 scans were collected to enhance the signal/noise (S/N) ratio and dynamic range.

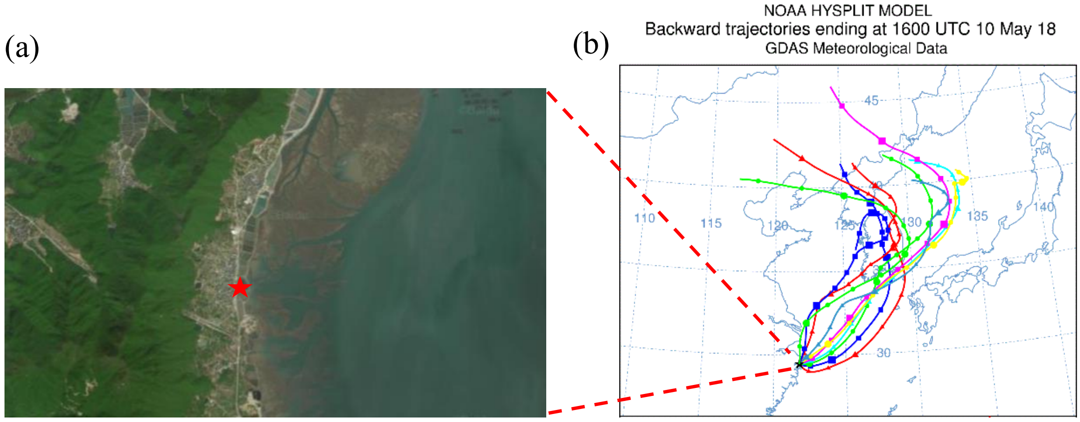

Figure S1. (a) The observation site, indicated as a red star, in an aerial photograph. Photo source: Baidu Map. (b) 72-hour air mass back trajectories ending at 100 m above ground level at the observation site computed by HYSPLIT model during the I-NPF events from My 8 to 10, 2018.

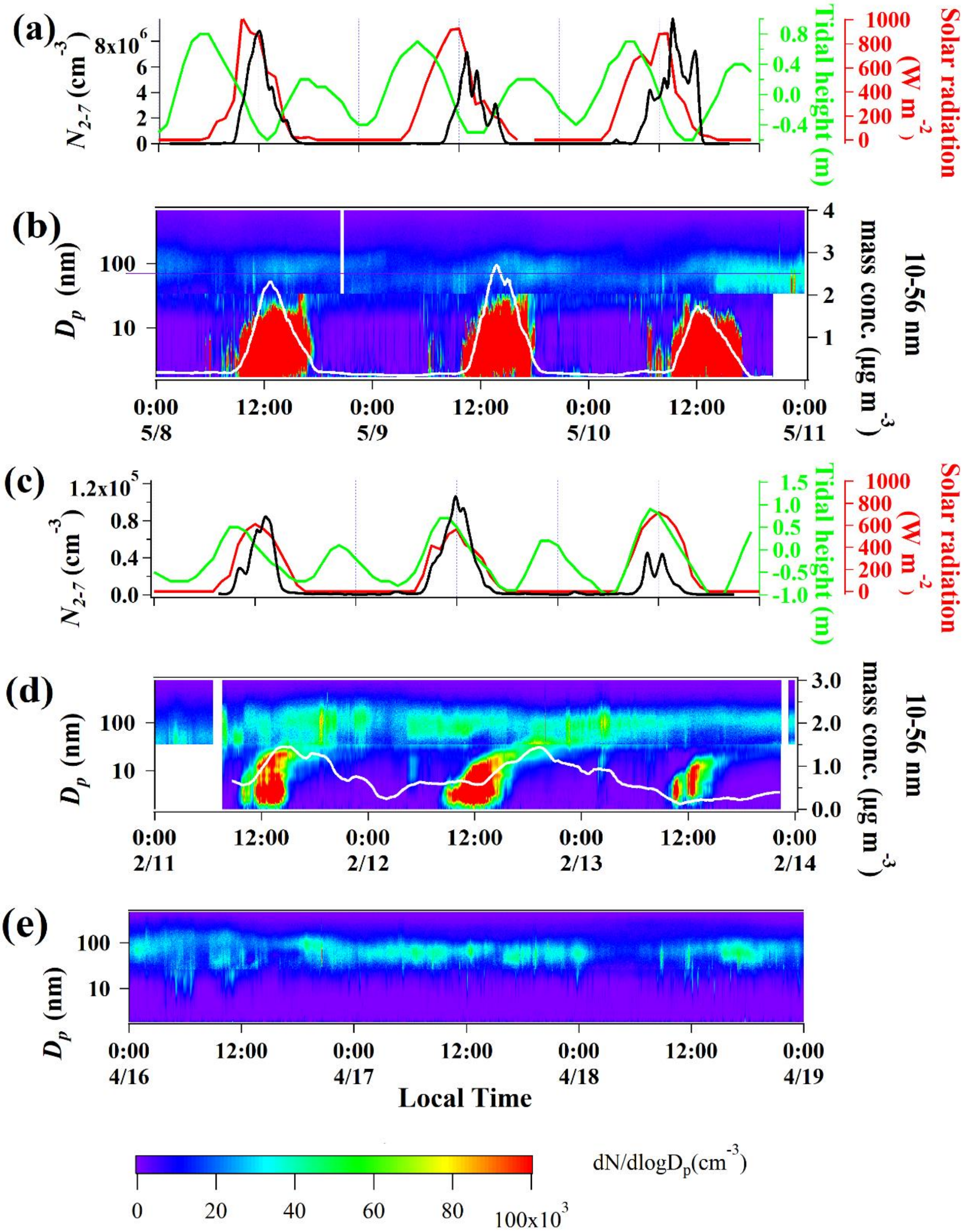

(a)
N_{2-7} (cm^{-3})
8x10^6
6
4
2
0
Tidal height (m)
0.8
0.4
0.0
-0.4
Solar radiation (W m^{-2})
1000
800
600
400
200
0
(b)
D_p (nm)
100
10
10-56 nm mass conc. (μg m^{-3})
4
3
2
1
0:00 5/8
12:00
0:00 5/9
12:00
0:00 5/10
12:00
0:00 5/11
(c)
1.2x10^5
0.8
0.4
0.0
N_{2-7} (cm^{-3})
Tidal height (m)
1.5
1.0
0.5
0.0
-0.5
-1.0
Solar radiation (W m^{-2})
1000
800
600
400
200
0
(d)
D_p (nm)
100
10
10-56 nm mass conc. (μg m^{-3})
3.0
2.0
1.0
0.0
0:00 2/11
12:00
0:00 2/12
12:00
0:00 2/13
12:00
0:00 2/14
(e)
D_p (nm)
100
10
0:00 4/16
12:00
0:00 4/17
12:00
0:00 4/18
12:00
0:00 4/19
Local Time
dN/dlogD$_p$(cm^{-3})
0
20
40
60
80
100x10^3

Figure S2. (a), (c) Number concentration of 2-7 nm particles ($N_{2\text{-}7}$), tidal height and solar radiation intensity during the Iodine-initiated NPF (I-NPF) days from May 9 to 11 and the continental regional NPF (C-NPF) days from February 11 to 13. Particle number size distribution and 10-56 nm particle mass concentration during (b) I-NPF days from May 9 to 11, (d) C-NPF days from February 11 to 13 and (e) non-NPF days from April 16 to 18.

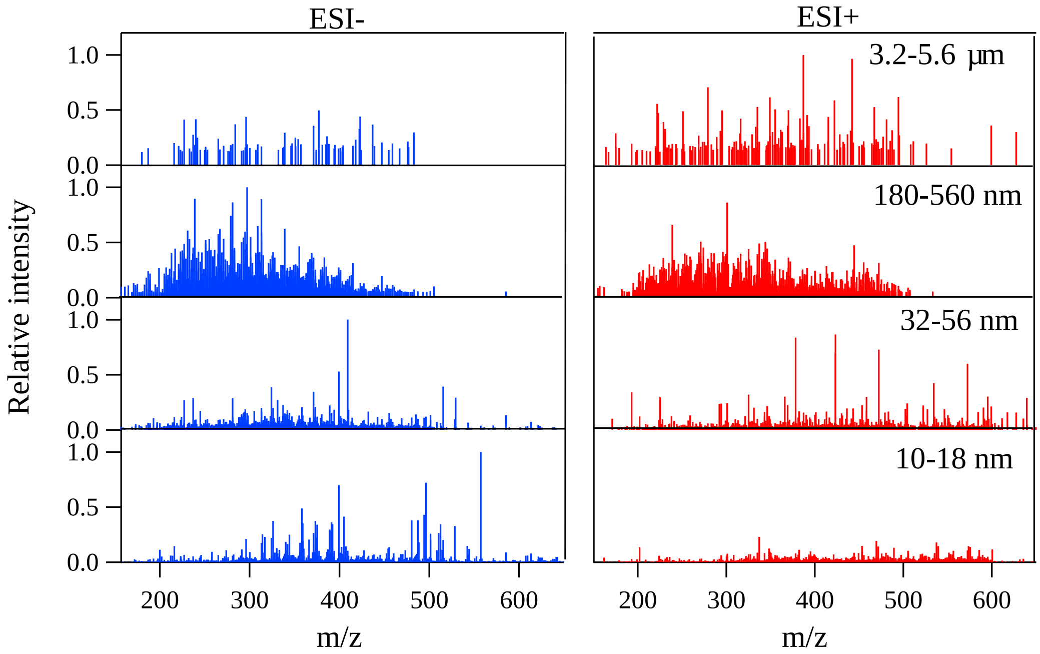

Figure S3. Reconstructed mass spectra of the 7 elemental groups in ESI- (left panels) and ESI+ (right panels) modes for the four size bins. The signals are normalized against the intensity of the most abundant molecular ions in a size bin.

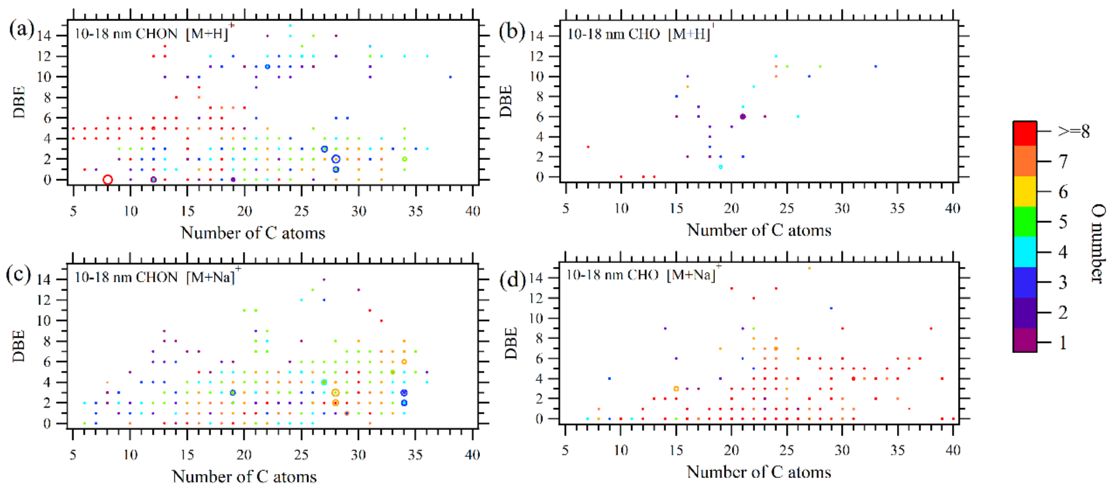

Figure S4. DBE vs. C atom number diagrams of all CHON and CHO formulas detected in 10–18 nm particles in ESI+ mode. (a) (b) $[M+H]^+$ adducts, (c) (d) $[M+Na]^+$ adducts. The color bar denotes O number in the formulas. The size of the circles reflects the relative intensities of molecular formulas on a logarithmic scale.

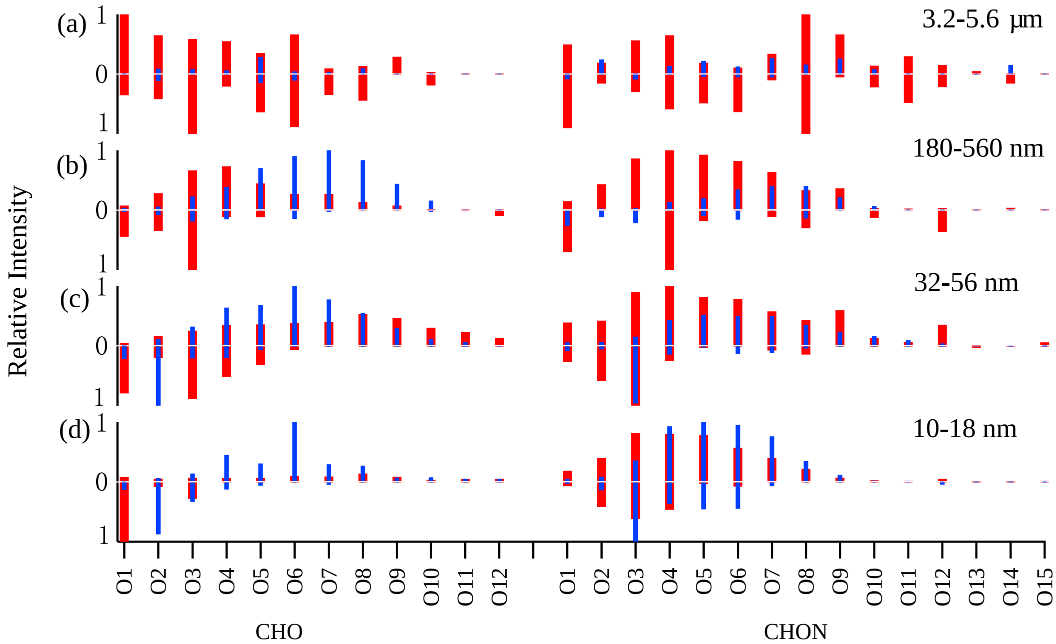

Figure S5. Relative intensities of subgroups according to O atom number in CHON, CHO, CHONI and CHOI formulas in the four size bins in ESI+ (in red) and ESI- (in blue). The intensity of the most abundant subgroup in a size bin is defined as 1 and those of other subgroups are normalized by it. The relative intensities of non-iodinated OC formulas (iodinated OC formulas) are plotted in the region above (below) zero line.

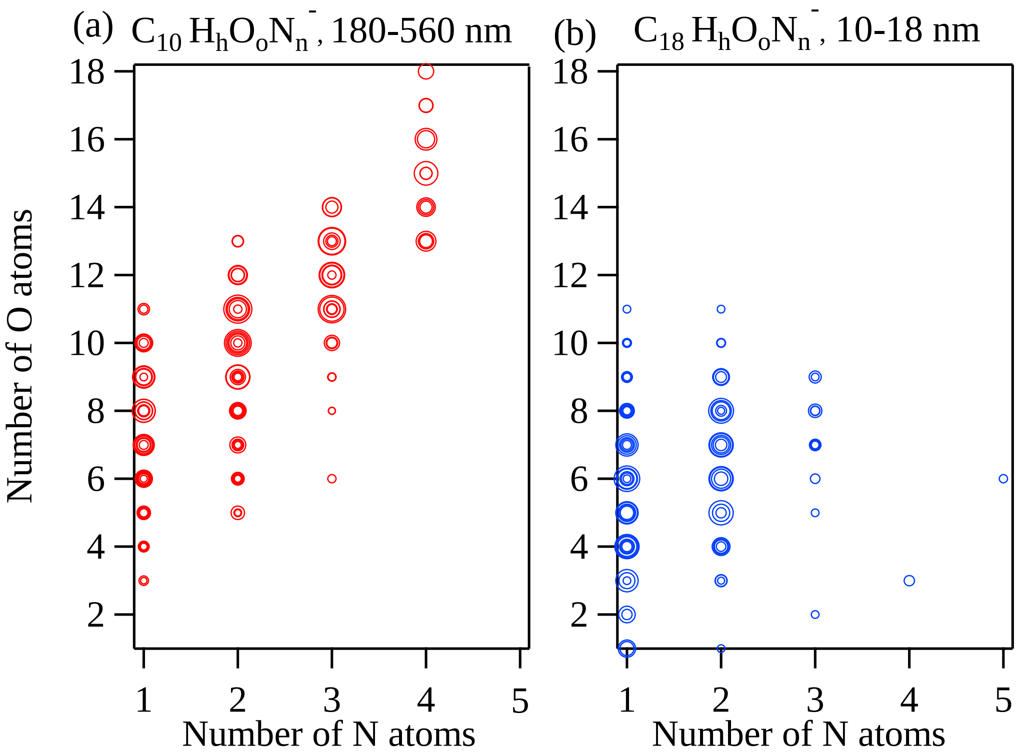

Figure S6. O atom number of *vs*. N atom number of $C_{10}H_hO_oN_n^-$ compounds detected in 180–560 nm particles (a) and $C_{18}H_hO_oN_n$- compounds detected in 10–18 nm particles in ESI- mode (b).

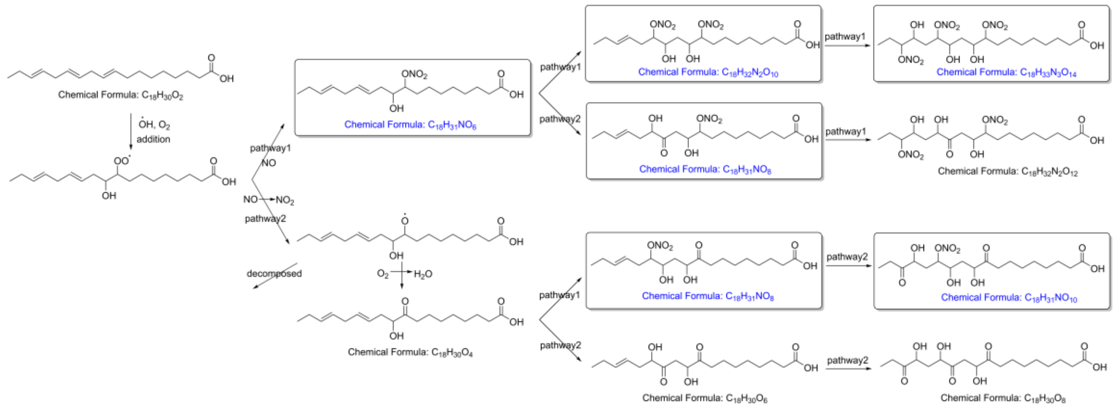

Figure S7. Simplified reaction scheme of the formation of oxygenated and nitrated CHO and CHON compounds from α-linolenic acid ($C_{18}H_{30}O_2$) oxidation in the atmosphere. One representative structure is shown for each chemical formula. Chemical formulas in the boxes are found in the formula list detected in 10–18 nm particles. Pathway 1: OH and O_2 addition followed by reaction with NO to form a –ONO_2 group; pathway 2: OH and O_2 addition followed by reaction with NO to form an alkoxy radical that further reacts with O_2 to form a –C=O group.

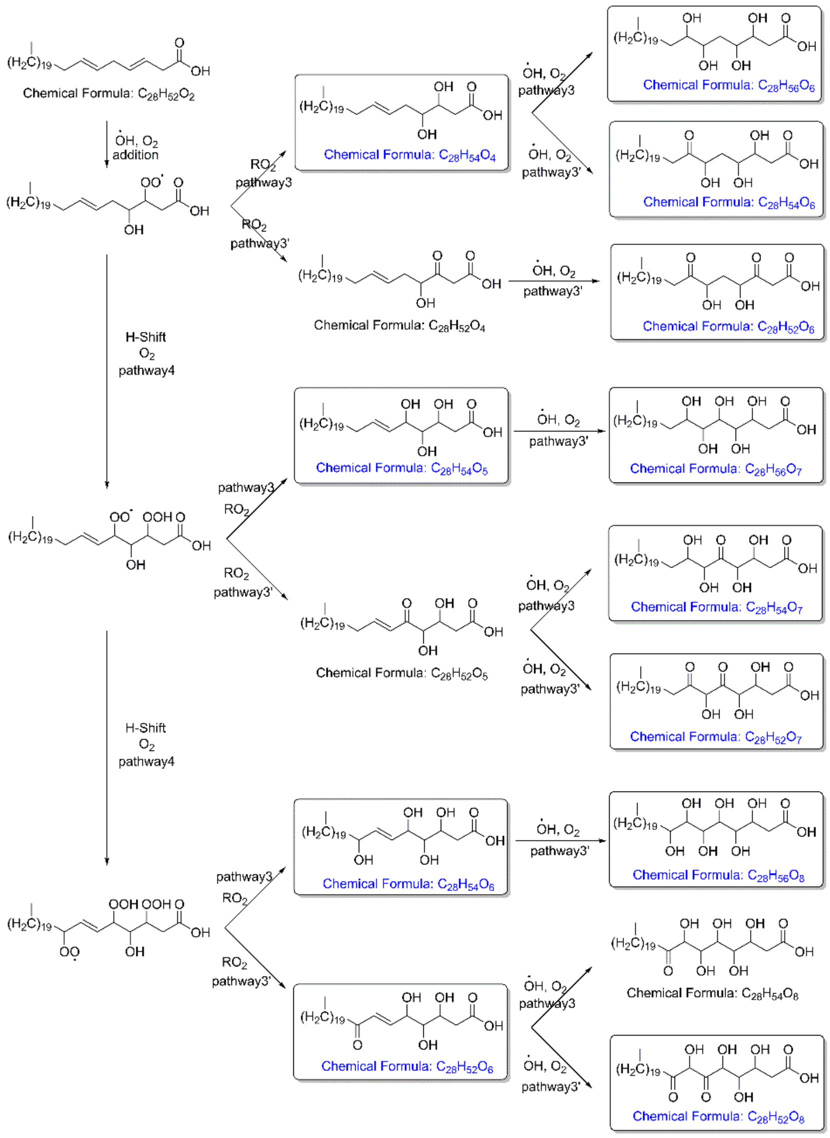

Figure S8. Simplified reaction scheme of the formation of oxygenated CHO compounds from unsaturated C28 FA ($C_{28}H_{52}O_2$) oxidation in the atmosphere. One representative structure is shown for each chemical formula. Chemical formulas in the boxes are found in the formula list detected in 10–18 nm particles. Pathway 3: OH and O_2 addition followed by reaction with RO_2 to form a –OH or a –C=O group; Pathway 4: successive intermolecular H-shift/O_2 addition (autoxidation) to form RO_2 radicals with –OOH group. –OOH group is not stable and decomposed to -OH.

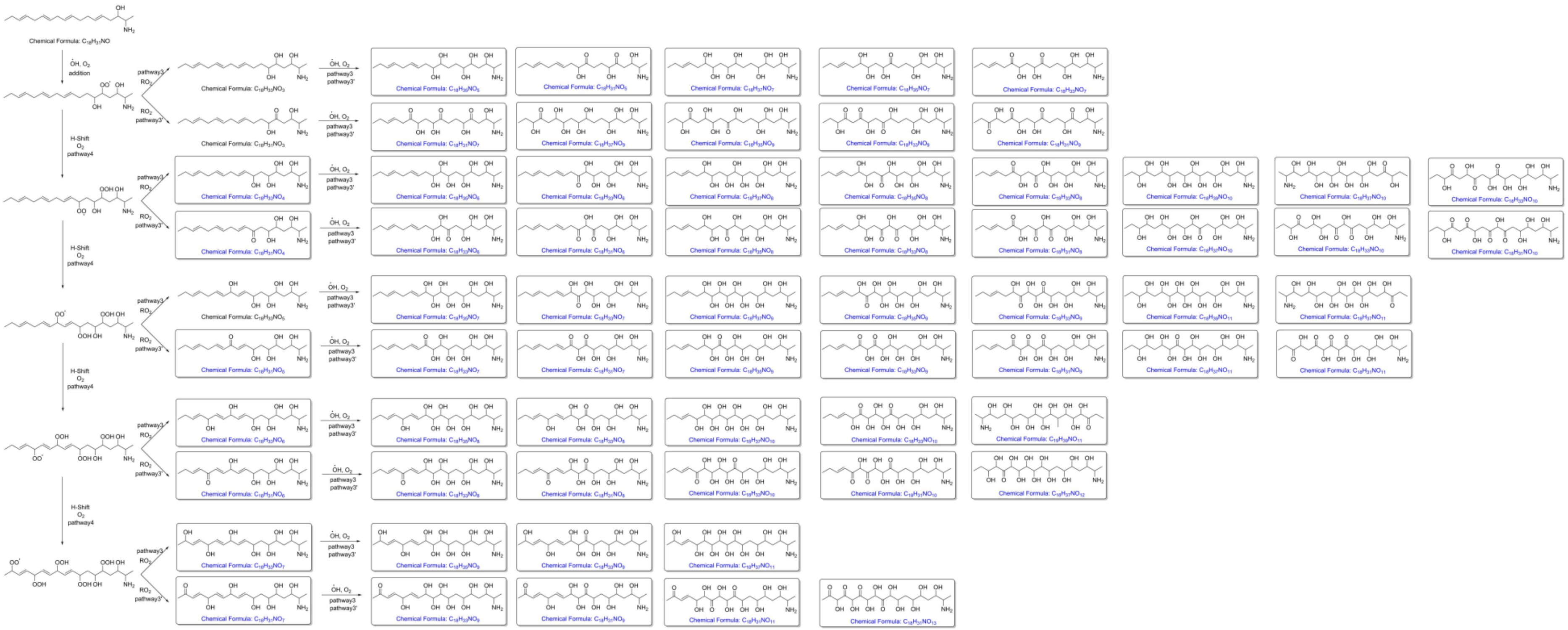

Figure S9. Simplified reaction scheme of the formation of oxygenated CHON compounds containing a –NH_2 group from unsaturated C_{18} amino alcohol ($C_{18}H_{37}NO_4$) oxidation in the atmosphere. One representative structure is shown for each chemical formula. Chemical formulas in the boxes are found in the formula list detected in 10–18 nm particles. Pathway 3: OH and O_2 addition followed by reaction with RO_2 to form a –OH or a –C=O group; Pathway 4: successive intermolecular H-shift/O_2 addition autoxidation to form RO_2 radicals with –OOH group.

Table S1. Predicted saturation concentration (C*) range of most abundant CHON and CHO formulas, as well as their possible precursors.

Formula	Predicted C^* (μg m^{-3})	Predicted C^* of possible precursors (μg m^{-3})
	ESI- mode	
$C_{18}H_{33}NO_4$	1.62×10^{-5}–2.06×10^{-2}	3.40×10^{-1}–8.91
$C_{18}H_{33}NO_6$	7.66×10^{-10}–1.33×10^{-2}	3.40×10^{-1}–8.87×10^{1}
$C_{18}H_{34}N_2O_6$	7.62×10^{-11}–1.32×10^{-3}	3.40×10^{-2}–8.91
$C_{18}H_{34}N_2O_7$	5.21×10^{-13}–9.06×10^{-6}	3.40×10^{-2}–8.91
$C_{18}H_{34}N_2O_8$	1.30×10^{-15}–5.56×10^{-6}	3.40×10^{-2}–8.91
$C_{18}H_{36}N_2O_5$	1.44×10^{-8}–1.10×10^{-2}	3.40×10^{-2}–8.87×10^{1}
$C_{18}H_{36}N_2O_6$	9.83×10^{-11}–7.54×10^{-5}	3.40×10^{-2}–8.87×10^{1}
$C_{18}H_{36}N_2O_7$	6.72×10^{-13}–5.15×10^{-7}	3.40×10^{-2}–8.87×10^{1}
$C_{19}H_{39}NO_7$	3.40×10^{-12}–1.15×10^{-7}	1.34×10^{-1}–3.51×10^{1}
$C_{30}H_{57}NO_4$	7.44×10^{-8}–6.69×10^{-6}	4.29×10^{-6}–1.16×10^{-3}
$C_{30}H_{59}NO_3$	5.58×10^{-9}–1.58×10^{-6}	4.29×10^{-6}–1.14×10^{-4}
$C_{30}H_{59}NO_4$	6.28×10^{-10}–8.62×10^{-6}	4.29×10^{-6}–1.16×10^{-3}
$C_{30}H_{59}NO_5$	4.52×10^{-12}–1.32×10^{-6}	4.29×10^{-6}–1.16×10^{-3}
$C_{30}H_{59}NO_6$	2.64×10^{-13}–8.93×10^{-9}	4.29×10^{-6}–1.16×10^{-3}
$C_{30}H_{60}O_6$	1.66×10^{-14}–3.76×10^{-13}	4.36×10^{-5}–1.16×10^{-3}
$C_{20}H_{40}O_6$	2.13×10^{-10}–4.83×10^{-9}	5.28×10^{-1}–1.39×10^{1}
$C_{21}H_{42}O_6$	8.32×10^{-11}–1.88×10^{-9}	2.07×10^{-1}–5.46×10^{0}
$C_{22}H_{44}O_4$	6.95×10^{-7}–1.57×10^{-5}	8.15×10^{-2}–2.15×10^{0}
$C_{24}H_{48}O_4$	1.06×10^{-7}–2.39×10^{-6}	1.25×10^{-2}–3.3×10^{-1}
$C_{26}H_{52}O_4$	1.60×10^{-8}–3.63×10^{-7}	1.90×10^{-3}–5.05×10^{-2}
$C_{27}H_{54}O_6$	2.87×10^{-13}–6.49×10^{-12}	7.42×10^{-4}–1.97×10^{-2}
$C_{28}H_{56}O_4$	2.41×10^{-9}–5.47×10^{-8}	2.89×10^{-4}–7.67×10^{-3}
$C_{28}H_{56}O_6$	1.11×10^{-13}–2.51×10^{-12}	2.89×10^{-4}–7.67×10^{-3}
$C_{29}H_{58}O_6$	4.29×10^{-14}–9.73×10^{-13}	1.12×10^{-4}–2.98×10^{-3}
$C_{33}H_{66}O_6$	9.56×10^{-16}–2.17×10^{-14}	2.54×10^{-6}–6.77×10^{-5}
$C_{38}H_{76}O_8$	3.66×10^{-22}–8.30×10^{-21}	2.18×10^{-8}–5.85×10^{-7}
	ESI+ mode	
$C_{11}H_{18}N_4O_8$	4.73×10^{-9}–3.63×10^{-3}	2.21×10^{0}–5.61×10^{2}
$C_{12}H_{20}N_4O_8$	1.85×10^{-9}–1.42×10^{-3}	8.85×10^{-1}–2.26×10^{2}
$C_{19}H_{35}NO_3$	9.26×10^{-4}	1.34×10^{-1}–2.23×10^{-1}
$C_{19}H_{36}N_2O_5$	4.35×10^{-9}–3.34×10^{-3}	1.34×10^{-1}–3.52×10^{0}
$C_{19}H_{37}NO_3$	1.20×10^{-3}–2.71×10^{-2}	1.34×10^{-1}–2.23×10^{-1}

$C_{19}H_{38}N_2O_3$	2.71×10^{-3}–5.04×10^{-3}	1.34×10^{-2}–3.52×10^{0}
$C_{24}H_{46}N_2O_4$	5.73×10^{-9}–4.39×10^{-3}	1.24×10^{-4}–3.28×10^{-2}
$C_{25}H_{43}NO_4$	3.07×10^{-7}–1.72×10^{-5}	4.83×10^{-4}–1.28×10^{-2}
$C_{26}H_{51}NO_5$	1.73×10^{-9}	1.88×10^{-4}–3.13×10^{-4}
$C_{27}H_{50}N_2O_4$	6.42×10^{-10}–3.29×10^{-7}	7.23×10^{-6}–1.95×10^{-3}
$C_{27}H_{50}N_2O_5$	3.11×10^{-11}–1.05×10^{-6}	7.23×10^{-6}–1.95×10^{-3}
$C_{27}H_{52}N_2O_3$	4.94×10^{-8}–2.76×10^{-6}	7.23×10^{-6}–1.95×10^{-3}
$C_{28}H_{52}N_2O_6$	1.14×10^{-14}–8.03×10^{-8}	2.81×10^{-6}–7.57×10^{-4}
$C_{28}H_{54}N_2O_6$	5.95×10^{-15}–1.03×10^{-7}	2.81×10^{-6}–7.57×10^{-4}
$C_{28}H_{56}N_2O_3$	6.09×10^{-8}–1.38×10^{-6}	2.81×10^{-6}–7.57×10^{-4}
$C_{28}H_{56}N_2O_6$	1.89×10^{-14}–5.88×10^{-9}	2.81×10^{-6}–7.57×10^{-4}
$C_{28}H_{58}N_2O_3$	3.18×10^{-8}	2.81×10^{-6}–4.66×10^{-6}
$C_{29}H_{56}N_2O_6$	2.30×10^{-15}–3.99×10^{-8}	1.09×10^{-6}–2.94×10^{-4}
$C_{29}H_{59}NO_7$	2.85×10^{-17}–6.47×10^{-16}	1.11×10^{-5}–2.94×10^{-4}
$C_{33}H_{59}NO_5$	1.05×10^{-12}–3.02×10^{-8}	2.49×10^{-7}–6.65×10^{-6}
$C_{34}H_{59}NO_6$	2.13×10^{-15}–1.38×10^{-9}	9.64×10^{-8}–2.57×10^{-6}
$C_{34}H_{66}N_2O_3$	1.15×10^{-11}–3.58×10^{-9}	9.45×10^{-9}–2.57×10^{-6}
$C_{34}H_{68}N_2O_3$	2.03×10^{-10}–4.61×10^{-9}	9.45×10^{-9}–2.57×10^{-6}
$C_{34}H_{68}N_2O_5$	3.75×10^{-15}–2.88×10^{-9}	9.45×10^{-9}–2.57×10^{-6}